Ionic organic-inorganic $(C_6H_{10}N_2)$ $(Hg_2Cl_5)_2.3H_2O$ compound: Structural study, Hirshfeld surface, thermal behavior and spectroscopic studies

Imen BEN SAAD [a,*] ; Najeh HANNACHI [a] ; Thierry ROISNEL [b] and Faouzi HLEL [a]

[a] Laboratory of spectroscopic characterisation and optics of materials, Faculty of Sciences, University of Sfax, B. P. 1171, 3000 Sfax, Tunisia.

[b], X-ray diffractometer Center. Rennes Institute of Chemical Sciences UMR 6226, CNRS , Rennes University 1, Beaulieu Campus, 35042, Rennes Cedex, France.

[*]**Corresponding author:** imen.bensaad.fss.2018@gmail.com

Abstract:

A novel organic-inorganic hybrid material $(C_6H_{10}N_2)(Hg_2Cl_5)_2.3H_2O$ has been prepared under hydrothermal conditions. It is characterized by single crystal X-ray diffraction, thermal analysis and spectroscopy measurements (IR, Raman and NMR). The structural analysis revealed that this material crystallizes in the monoclinic system (*C 2/c* space group*)* with the following unit cell parameters a = 19.6830(15) Å, b =18.1870(15) Å, c = 6.8567(6) Å, β = 93.224(3) ° and Z=4. According to the data collected at 150(2) K, the refinement converged to R= 0.0296. The atomic arrangement can be described as an alternation of cationic $[C_6H_{10}N_2]^{2+}.H_2O$ and anionic $[Hg_2Cl_5]^-$ layers along the *c* axis. In fact, a three-dimensional cohesion, which leads to these peridinium complexes, involves (N-H***Cl) (N-H***O) (O-H***O) and π–π interactions. Furthermore the FT-IR, Raman and NMR-MAS confirm the presence of organic and inorganic entities. Finally, the differential scanning calorimetry revealed several endothermic peaks.

Keywords: Organic-inorganic hybrid; X-ray diffraction; Hirshfild surface; FT-IR; FT-Raman spectroscopy and NMR.

1. Introduction

The advancement of recent technology and the need for new functions are generating a huge demand for new materials and new applications **[1-7].** For this reason, organic-inorganic hybrid materials are receiving attention because they can help combine the specific properties of inorganic frameworks and futures of organic molecules **[8, 9].** Recently, much attention has

been paid to organic-inorganic hybrid materials based on metal-halide units. Indeed, the synthesis of low-dimensional inorganic-organic materials enables both inorganic and organic components at the molecular level to be optimized. The organic cations, which are characterized by a special kind of π- π interaction in aromatic ring compounds, have attracted attention NLO materials; there are many typical aromatic that shows interesting photochemical properties **[10-12].**

In particular, hybrid materials based on ammonium and metal divalent (Cd, Zn, Hg ...) halides used a solvent in the synthesis of a large number of chemicals in various classes. The structural chemistry of Cd (II), Zn (II), Hg (II) or Cu (II) halides in the solid state is exceptionally diverse, which can provide electrical mobility **[13-15].** Among the systems that are currently receiving a limited attention are the Hg-based halides. Since the states around the Fermi level in organic-inorganic halide hybrid materials (HOIMs) are dominated by metal and the halogenated states, the Hg-based compounds should have band gaps compared to Cd and Zn hybrids due to the difference in electro negativity of Hg halide metal **[16-17].** Mercury (II) is the most volatile material. The flexibility of mercury (II) makes it possible to form octahedral and tetrahedral complexes. All the properties are related to the structural changes of these compounds, depending on the effects of different factors, such as temperature and composition. The mercury complex shows a wide range of coordination numbers and geometries (tetrahedral, trigonal, bipyramidal and octahedral), because of the relatively closed shell of the large coordination distances of Hg (II) in the compounds. For this reason, the crystal structure arrangement is appreciably different **[18-20].** All the properties are related to the structural change of this compound, depending of the effects of the different factors, such as temperature and composition **[21-24]**.

In this context, we are going to report in the present paper the synthesis of $(C_6H_{10}N_2)(Hg_2Cl_5)_2.3H_2O$ through a hydrothermal method. We have performed X-ray diffraction measurements which provided us with information about the complete crystal structure at 150(2) K of the new compound. The Hirshfeld surface analysis is introduced in order to evaluate the interactions within the crystal structure. This structural study is accompanied by thermal analyses and spectroscopic study (RAMAN; IR; NMR-MAS) measurements.

2. Methodology

2.1. Experimental details

2.1.1. Synthesis

The single crystal of the title compound $(C_6H_{10}N_2)(Hg_2Cl_5)_2.3H_2O$ was prepared by hydrothermal methods as follows: 1, 2-benzen diammonium $C_6H_8N_2$ (0.0905 g; 0.836 mmoles;67.5%) and mercury chloride $HgCl_2$ (0.9094 g;3.349 mmoles;32.5%) were dissolved in aqueous solution of HCl (2M; 37%) for a few minutes with agitation successive to ensure complete dissolution of the compound. Second, such solutions were slowly combined in an autoclave and kept at 85 °C under auto-genous pressure for 24 h. After cooling these solutions for five days at room temperature, colourless single crystals suitable for an X-ray structure determination were obtained. Schematically the reaction is shown in the following equation:

$$C_6H_8N_2 + 4\,HgCl_2 \xrightarrow[\text{diluted}]{\text{HCl}} (C_6H_{10}N_2)(Hg_2Cl_5)_2.3H_2O$$

2.2.2. Crystal structure determination

The X- ray diffraction data collection was performed using a single crystal (0.150 x 0.120 x 0.090 mm) selected through an optical examination. Intensity data were obtained on a D8 VENTURE Bruker AXS diffractometer equipped with a (CMOS) PHOTON 100 detector using Mo Kα radiation (λ= 0.71073 Å, multilayer monochromator). The data were collected at 150(2) K. The compound crystallizes in the monoclinic system with *C* 2/*c* space group. The basic crystallographic data and the details of the measurements and refinement are summarized in table 1. The structure was solved by means of a dual-space algorithm using the *SHELXT* program **[25],** and then refined with full-matrix least-square methods based on F^2 (*SHELXL*) **[26].** All the non-hydrogen atoms were refined with anisotropic atomic displacement parameters. H atoms were finally included in their calculated positions and treated as riding on their parent atom with constrained thermal parameters. A final refinement with 2805 unique intensities and 117 parameters converged to ωR (F^2) = 0.0710 and R (F) = 0.0296) for 2667 observed reflections with I > 2σ(I). The fractional atomic coordinates and equivalent isotropic displacement parameters ($Å^2$) are presented in table 2.

2.3. Hishfeld surfaces

The inter contacts observed in the crystal structure are quantified and graphically visualized using Hishfeld surface computational method. Here, we estimate the intermolecular interactions through inter contacts and then, we discuss the results.

2.4. Spectroscopy measurements (IR, Raman and NMR-MAS)

The infrared spectrum was recorded in the 400–4000 cm^{-1} range with a *Nicolet IR 200 FT* 1000 spectrometer using a sample pressed in spectroscopically pure KBr pellets.

Back scattering Raman spectra were obtained under microscope with a HR 800 Raman spectrometer (Horiba Jobin-Yvon) with nitrogen cooled CCD detector. The spectra were registered in two acquisitions from 50 to 3500 cm^{-1}.

The NMR-MAS experiments were performed at room temperature on a Bruker WB 300. Then, the powdered sample was packed in a 4 mm diameter rotor and set to rotate at a speed of 8 kHz in a Doty MAS probehead. The ^{13}C spectrum was collected through a cross-polarization of proton with 5 ms contact time.

2.5. Thermal behavior

A thermogravimetric analysis (TGA) was carried out using an ATG PYRIS 6 instrument at the temperature range from 303 to 773 K with a heating rate of 10°C/min under a nitrogen atmosphere. The Differential Scanning Calorimeter (DSC 400) was used to examine the phase behavior of the $(C_6H_{10}N_2)(Hg_2Cl_5)_2.3H_2O$ salt. The spectrum was obtained from temperature sweep experiments by heating the mixed system 303-443 K at the rate of 10°C/ min. The sample was weighed into aluminum pans, and the covers were crimped into place. Prior to the sample analysis, the baseline was obtained with an empty, hermetically-sealed aluminum pan.

3. Results and discussion

3.1. Structural analysis and Geometry optimization

The asymmetric unit of the title compound (Fig.1) is made up of one inorganic $(Hg_2Cl_5)^-$ anion, a half $(C_6H_{10}N_2)^{2+}$ cation and two water molecules (H_2O). In fact**,** the projection along the *c* axis of the atomic arrangement can be described by the alternation of cationic and

anionic layers. The cohesion of compound entities is ensured by hydrogen bonding (N-H***Cl), (N-H***O), (O-H***O) and π–π interactions (Fig .2).

The cationic layer (Fig .3) is formed by $(C_6H_{10}N_2)^{2+}$ groups observed at *z/b* = 1/3. Between organic entities, two water molecules are intercalated. Each two cations are antiparallel, managed by inversion center while orienting their groups (NH_2) towards the inside and outside layers to establish weak hydrogen bonds N-H***Cl with adjacent anionic layers and N-H***O with water molecules. The value of the centroid-to-centroid distances between the two $(C_6H_{10}N_2)^{2+}$ rings averaging 4.3 Å, This value indicates a rather weak π–π interaction **[27].** The atoms of all the organic cations will be differentiated by their position in the plan as well as their directions of the ammonium groups. The C-C bond lengths vary from 1.378 (10) Å to 1.402(13) Å and the C-N bond length value is equal to 1.467(9) Å. On the other hand, the coordination around $(C_6H_{10}N_2)^{2+}$ cation is characterized by two different sets of N-H***O cohesion with two short N-H bonds (≈ 0.910 Å). However, the C-C-C, C-C-N angles are in the range of 119.80(4) ° to 120.50(7) ° and 119.20(6) ° to 120.90(4) °, respectively (table. 3). The Bond length and angle values are in good agreement with the bond lengths of the other aromatic salts **[28-31]**.

As far as the geometry of the dimeric of $(Hg_2Cl_5)^-$ anions (Fig .4) is concerned, $(Hg_2Cl_5)^-$ is an assembly of two in-equivalent triangles determined by the association of two monomercury chloride $HgCl_3^-$ units which carry a chlorine atom- common $Cl_{(3)}$. Hg atoms are three coordinated as to built two triangles linked via $Cl_{(3)}$ chlorines atoms. The linkage (L) (Hg-Cl_L) bonds Hg-$Cl_{(3)}$, 2.7985(17) Å to 2.856(2) Å are greater than the external (E) (Hg-Cl_E) ones. The last distances are around 2.335(2) Å (table 4). In both triangles, Cl_E-Hg-Cl_E are greater than the ideal values (120°), as they are 163.22 (7) ° in $Cl_{(2)}$-$Hg_{(1)}$-$Cl_{(1)}$ and 161.93 (7) ° for $Cl_{(5)}$-$Hg_{(2)}$-$Cl_{(4)}$. The Cl_L-Hg-Cl_E angles are smaller than the ideal values (120°) as they vary between 90.07 (6) ° and 99.85 (6) °.

The $Hg_{(1)}Cl_3$ triangle is planar and <Cl-Hg-Cl> is close to 120°. However, the $Hg_{(2)}Cl_3$ triangle is pseudo-planar and <Cl-Hg-Cl> equal to 117° and Hg atom is looked out chlorine atoms plane. Booth $HgCl_3$ triangles are not coplanar but they show a decaled representation. The $Hg_{(2)}$-$Cl_{(3)}$-$Hg_{(1)}$**,** which is equal to 132.44 (6) °, is significantly characterized by the presence of two types of $(Hg_2Cl_5)^-$. The great value bond length of Hg –Hg found for the distance between the two mercury atoms is considerably larger than the expected Van Der Waals contacts. This result is comparable to the reported compound**s**. The $(Hg_2Cl_5)^-$ anionic species has been frequently observed in mercury halide chemistry **[29, 32-39].** The $(Hg_2Cl_5)^-$ - $(C_6H_{10}N_2)^{2+}$-H_2O –$(Hg_2Cl_5)^-$ molecular unit is built through the formation of N(O)-H***O

and N(O)-H***Cl hydrogen bonds from nitrogen or oxygen atoms on the chlorine atoms in the anions.

In fact, there are several types of hydrogen bonding interactions present in the crystal structure. These interactions provide a linkage between the cationic $(C_6H_{10}N_2)^{+}$ entities and $(Hg_2Cl_5)^{2-}$ anions. The bonding between inorganic and organic entities in the compounds is realized by two types of hydrogen bonding N-H***Cl and N-H***O reported in (table.5) and showed in (fig.5). The N-Cl distances vary between 3.134(4) Å and 3.691(4) Å. In this compound, the H-Cl and H-O distances are in the range of 1.91 Å to 2.87 Å and 2.76(1) Å to 3.390(8) Å, respectively. However, the N-H***Cl and N-H***O angle values vary from 117.5°–177.6° to 140.5°–160.7°, respectively.

The type and the number of hydrogen bonds around each $(Hg_2Cl_5)^{-}$ anion are strongly influenced by the position of the aromatic ring. In fact, two different types of hydrogen bond are found. The aromatic cation inherently possesses the ability to approach the anion without steric hindrance and can therefore share its N-H proton with the chlorine atom commun acceptors. The chlorine atom is involved in hydrogen bond interactions with cation. The N-H distances are approximately equal to 0.910 Å, suggesting that the $(C_6H_{10}N_2)^{2+}$ cations have established two nearly symmetric hydrogen bonds. The material cohesion is assured by two different interactions**,** which may indicate a reasonably low interaction **[40-41].**

3.2. Study of intermolecular interactions through Hirshfeld surface analysis

The identification and the visualization of the intermolecular short/long contacts are determined in the reported structure by means of the powerful Hirshfeld surface analysis technique. This method is constructed based on the electron distribution calculated as the sum of spherical atom electron densities **[42-43].** Hirshfeld surfaces and their associated two-dimensional fingerprint plots (2D) are calculated using CRYSTAL EXPLORER 3.1 software **[44].** The breakdown of the two-dimensional fingerprint plots was used for identification of the regions of particular importance to intermolecular interactions by color-coding having short or long contacts **[45].** In this study, the Hirshfeld surfaces treat molecular interactions in cells and it's defined by points where the contribution to the electron density from the molecule of interest is equal to the contribution from all the other molecules. For a given crystal structure and set of spherical atomic electron densities, the combination of d_e (the nearest nucleus outside the surface) and d_i (the nearest nucleus inside the surface) in the form of a 2D fingerprint plot provides a summary of intermolecular contacts in the crystal.

The d_{norm} (normalized contact distance) is a symmetric function of distances from the Hirshfeld surface (d_i) and (d_e) were the first functions of distance explored for mapping on the surfaces, relative to their respective *Van Der Waals radii* of the atoms internal or external to the surface (r_i^{vdw} / r_e^{vdw}) which identifies the regions of particular importance to the intermolecular interactions. Complementary regions are also visible in the fingerprint plots where one molecule acts as a donor ($d_e > d_i$) and the other as a recipient ($d_e < d_i$) (table 6). The 2D fingerprint plots presented in this paper were generated using the reported equation (1) in **[46-47].**

Eq.1: $d_{norm} = \frac{d_i - r_i^{vdw}}{r_i^{vdw}} + \frac{d_e - r_e^{vdw}}{r_e^{vdw}}$

The 2D fingerprint maps of $(C_6H_{10}N_2)$ $(Hg_2Cl_5)_2.3H_2O$ provide some quantitative information about the individual contribution of the intermolecular interaction in the asymmetric unit Fig6, and some distinct spikes appearing in the 2D fingerprint plot which estimate the different interaction motifs in the crystal lattice Fig. 7

The major contribution is from Cl-H (11.8%), H-Cl (8.7%) (e). This is evidence that van der Waals forces exert an important influence on the stabilization of the packing in the crystal structure, while other intercontacts contribute less to the Hirshfeld surfaces: C-C (5.4%) (b), H-C/C-H 1.4%/2.4% (f); H-O (4.5%) (j) H-H – 3.3 % (i) and O-O 3.5%(k). However, the Cl-Cl (d) and Hg-Cl (g) contacts have significant contributions, 11.3 %, and 11.7% % respectively. Again, very low percentages of Hg-Hg and Cl-C/C-Cl (0.4%) (a) and (0.9%)/(0.7%) (h) respectively interactions are recorded in the molecule.

3.3. Infrared and Raman spectroscopy

In order to identify the results obtained by means of the crystal structure description of the cationic-anionic layers of the functional groups were studied the vibrational spectroscopy. Therefore, we have investigated the vibrational properties of the organic and inorganic groups using the Raman scattering and infrared absorption at room temperature. Fig.8. (a), presents the IR and Raman spectra of the reported compound at room temperature. The assignments of the observed bands**,** which are based on a comparison of the modes and frequencies observed in similar compounds **[14, 31, 48-51]**, are listed in table 7.

It should be noted that the region high-frequencies 3400 cm^{-1} and 3350 cm^{-1} in IR are related to the symmetric and asymmetric stretching of (OH). Furthermore, the bands observed at 3235 cm^{-1} and 3280 cm^{-1} in IR are ascribed to symmetric and asymmetric stretching of NH. Those observed at 3157 cm^{-1} and 2360 cm^{-1} in IR are assigned to the symmetric and asymmetric stretching of CH. The band located around 1670 cm^{-1} in IR is attributed to the stretching of C=C. The bands observed at 1369 cm^{-1} and 1473 cm^{-1} in infrared correspond to scissoring of CH + NH as well as to the stretching of CN. However, the bands located at 1257 and 1290 cm^{-1} in FT-IR and at 1070 cm^{-1} in Raman are assigned to the stretching vibration of C=N. Nevertheless, the (C-C) bending out-of-plane wavenumbers are assigned at 1112 cm^{-1} in infrared, while the NH wagging mode observed at 689 cm^{-1} in IR and at 601 cm^{-1} in Raman. In fact, the C-C-N in the plane-bending vibration is observed at 591 cm^{-1} in infrared and in Raman at 567 cm^{-1}. Finally, the C=C bands show a scissoring vibration at 429 cm^{-1} and at 432 cm^{-1}. The wavenumbers observed with precision of the Raman lines are determined by using the LabSpec5 program with a combined Lorentzian-Gaussian band (fig.8.b). The error range for the determination of the peak position is ±0.5 cm^{-1} after the accumulation of the data and fitting procedure.

This study is limited to the low-frequency range (50 to 450 cm^{-1}), because it includes some lattice and internal modes which are very sensitive to crystal changes and phase transitions **[14].** The Raman lines observed at 55 cm^{-1} are associated with the anionic $(Hg_2Cl_5)^-$ layers. The shoulder at 100 cm^{-1} and the band at 110 cm^{-1} correspond to the $HgCl_2$ libration of the layers. A well resolved band at 237 and 250 cm^{-1} corresponds to υ Hg–Cl **[52].**

3.4. CP/MAS-NMR spectroscopy

The NMR spectrum ^{13}C CP–MAS of the title compound rotating at magic angle and set to rotate at a speed of up to 8 kHz is shown in Fig.9.

The simulation of these NMR-MAS spectrum isotropic bands is carried out using the Dmfit solid-state NMR spectroscopy program **[53]**. The spectrum is composed of three isotropic bands b_1, b_2 and b_3 with different ppm.

The simulation of the isotropic band permits to identify six peaks using Gaussian and Lorentzian functions (table 8). The deconvolution of signal b_3 shows the presence of two resonances observed at 121, 123 ppm correspond C_3 and C_4 carbon atoms. Signal b_2 shows the existence of two resonance at around 128, 129 ppm which can be attributed to C_2 and C_5 **[54]**. The most shielded signal b_1, which is located at 131, 133 ppm, corresponds to the carbon

atoms C_1 and C_6 linked to the nitrogen atoms **[55, 56]**. The remainder chemical shift, the values of which are commonly observed in similar compounds **[57],** corresponds to the aromatic carbon atoms of the phenyl ring. In an X-ray single crystal study, the cation present C_v poncutel symmetry and carbon atoms occupy three in-equivalent sites. Inversely, the NMR-MAS measurements permit to localize six in-equivalent carbon sites. However, the NMR technique is more sensible to electronic density neceilies which is influenced by H bonding in this case.

3.5.Thermal analysis

The resultats of the calorimetric (DSC) and the thermogravimetric (TGA) measurement for $(C_6H_{10}N_2)(Hg_2Cl_5)_2.3H_2O$ are illustrated in Fig.10. The endothermic peak, observed on the DSC curve at 336 K, is accompanied by weight loss equal to 2.835% (weight loss calculated 2.725%) on the TGA curve. This corresponds to the departure of two molecules of water. After that, the monohydrate compound $(C_6H_{10}N_2)(Hg_2Cl_5)_2.1H_2O$ appears to be stable up to about 355K. Above this temperature several endothermic peaks found by DSC accompanied with a major loss weight indicating the decomposition of the material.

4-Conclusion

This manuscript reports a new mercury (II) hybrid which is a new compound that has been synthesized under hydrothermal conditions and characterized by a single-crystal X-ray diffraction, Hirshfeld surface analysis, spectroscopic study and thermal behavior. Their structure contains a half $[C_6H_{10}N_2]^{2+}$ cation and inorganic $[Hg_2Cl_5]^-$ anion. The crystal crystallizes in the monoclinic system with *C 2/c* space group at 150 K, besides, its structural arrangement can be described as an alternation of organic-inorganic layers, which is performed via (O–H…..Cl), (N–H…O),(O–H…O) between anions and cations and π–π stacking interactions established between parallel cations. The vibrational proprieties of this compound are studied by means of Infrared and Raman Spectroscopy which confirms the presence of organic and inorganic groups. Moreover, the ^{13}C NMR spectra revealed that the presence of six resonances corresponds to the six carbon atoms of the organic cation. The thermal investigation of the title crystal structure indicates conformity between the results presented by TGA and DSC.

5. Supplementary material

Crystal data for a new complex containing: $(C_6H_{10}N_2)$ $(Hg_2Cl_5)_2$ $3H_2O$, has been deposited at the Cambridge Crystallographic Data Center as supplementary publications (CCDC - 1836685). The data can be obtained free of charge at http://www.ccdc.cam.ac. uk/conts/retrieving.html or from the Cambridge Crystallographic Data Center, 12 Union Road, Cambridge CB2 1EZ, UK; fax: 44 1223 336 033; E-mail: deposit@ccda.cam.ac.uk.

REFERENCES

[1] W.P. Wu, P. Liu, Y.T. Liang, L. Cui, Z.P. Xi, Y.Y.Wang,Journal of Solid State Chemistry, 2015,228 ,124-130.

[2] W.W. Lestari, H.C. Streit, P. Lonnecke, C. Wickleder, E. Hey-Hawkins, Journal of Dalton Transactions, 2014,43 ,8188- 8195.

[3] D.F.S. Gallis, L.E.S. Rohwer, M.A. Rodriguez, T.M. Nenoff, Journal of Chemistry of Materials,2014, 26, 2943- 2951.

[4] H. He, F. Sun, T. Borjigin, N. Zhao, G. Zhu, Journal of Dalton Transactions, 2014, 43, 3716-3721.

[5] P.F. Wang, Y. Duan, J.M. Clemente-Juan, Y. Song, K. Qian, S. Gao, L.M. Zheng, Journal of Chemistry - A European Journal,2011,17, 3579- 3583.

[6] S. Hu, L. Yun, Y.-Z. Zheng, Y.-H. Lan, A.K. Powell, M.-L. Tong, Journal of Dalton Transactions, 2009,11,897.

[7] M.A.M. Abu-Youssef, A. Escuer, F.A. Mautner, L. Öhrström, Journal of Dalton Transactions, 2008,27,3553.

[8] R.M. Laine, C. Sanchez, C.J. Brinker, E. Gianellis,Organic/Inorganic Hybrid Materials,Materials Research Society Series, 2000,628.

[9] C. Sanchez, B. Lebeau, in: D.A. Loy (Ed.), Materials Research Society Bulletin, 2001,26, 377-387.

[10] J. Dai, G. Bian, X. Wang, Q. Xu, M. Zhou, M. Munakata, M. Tong, Z. Sun, H. Zeng,

Journal of the American Chemical Society, 2000, 122, 11007- 11008.

[11] Y. Ji, J. Zuo, L. Chen, Y. Tian, Y. Song, Y. Li, X. You ,Journal of Physics and Chemistry of Solids, 2005,66, 207- 212.

[12] Y. Cheng, Y. Mao, J. Liu, S. Feng, T. He, Journal of Modern Optics, 2007, 54, 2763-2768.

[13] R. Elwej , M. Hamdi, N. Hannachi, F. Hlel, Journal of Spectrochimica Acta Part A, 2014 ,121, 632- 640.

[14] F. Zouari , A.Ben Salah, Journal of Solid State Sciences, 2004, 6, 847- 851.

[15] N. Salah, B. Hamdi, N. Bouzidia, A. Ben Salah, Journal of Molecular Structure, 2017,1149, 414- 425.

[16] A. Allred, Electronegativity values from thermochemical data, Journal of Inorganic and Nuclear Chemistry, 1961,17, 215- 221.

[17] G. Wulfsberg, 'Principles of Descriptive Inorganic Chemistry', University Science Books, Mill Valley, CA, 1991, 393.

[18] J. Malito, Journal of Annu. Rep. Prog. Chem., Sect. A: Inorg.Chem, 2002, 98, 115- 128.

[19] I. B. Gorrell, Journal of Annual Reports Section "A" (Inorganic Chemistry) ,1998,94, 137.

[20] W. Levason ,C. A. McAuliffe, The Chemistry of Mercury, 1977,60 ,47-135.

[21] I.D. Giles, H.T. Chifotides, M. Shatruk, K.R. Dunbar, Journal of Chemical Communications, 2011, 47, 12604.

[22] H.T. Chifotides, I.D. Giles, K.R. Dunbar, Journal of the American Chemical Society , 2013,135 3039 -3055.

[23] H.T. Chifotides, K.R. Dunbar, Journal of Accounts of Chemical Research,2013,46, 894-906.

[24] C.S. Campos-Fernández, B.L. Schottel, H.T. Chifotides, J.K. Bera, J. Bacsa, J.M. Koomen, D.H. Russell, K.R. Dunbar, Journal of the American Chemical Society, 2005,127, 12909- 12923.

[25] G.M.Sheldrick, Journal of Acta Crystallographica Section C, 2015, A71, 3-8.
[26] G.M .Sheldrick, Journal of Acta Crystallographica Section C, 2015, C71, ,3-8.

[27] B. Kulicka, R. Jakubas , Z. Ciunik, Journal of Solid State Sciences,2006, 8 , 1229- 1236

[28] M. Belhouchet, W. Wamani, T. Mhiri, Journal of IOP Conference Series: Materials Science and Engineering, 2010, 13,012039.

[29] M. Amami, S. V. Smaalen, A. Ben Salah, X.Helluy, A. Sebald, Journal of Solid State Chemistry,2004,177,2961- 2970.

[30] A.Jellibi, I. Chaabane, K.Guidara,Journal of Polyhedron, 2015, 89, 11-18

[31]I.Mkaouar,N.Karâa, B. Hamdi, R. Zouari, Journal of Molecular Structure,2016,1115,161-170.

[32] Chloromercury (II)anions,Journal of Coordination Chemistry Reviews ,1994,135-136-136, 533- 586.

[33] P.R. Bontchev, B.B. Ivanova, R.P. Bontchev, D.R. Mehandjiev, Journal of Polyhedron,2001,20, 231- 236.

[34] N.S. Herringer, M.M. Turnbull, C.P. Landee, J.L. Wikaira, Journal of Dalton Transactions, 2011,40,4242.

[35] R. Elwej, M. Hamdi, N. Hannachi, F. Hlel,Journal of Materials Research Bulletin, 2015,62, 42- 51.

[36] I.D. Brown,Journal of Acta Crystallographica Section A, 1976,32, 24-31.

[37] A.R. Parent, C.P. Landee, M.M. Turnbull, Journal of Inorganica Chimica Acta ,2007,360, 1943-1953.

[38] K. Edwards, S.N. Herringer, A.R. Parent, M. Provost, K.C. Shortsleeves, M.M. Turnbull, L.N. dawe. Journal of Inorganica Chimica Acta, 2011,368, 141-151.

[39] A. Kessentini, M. Belhouchet, Y. Abid, C. Minot, T. Mhiri, Journal of Spectrochimica Acta Part A,2014,122,476-481,.

[40] S. Banerjee, A. Ghosh, B. Wu, P. G. Lassahn, C. Janiak, Journal of Polyhedron, 2005,24, 593- 599.

[41] F. Neve, O. Francescangeli, A. Crispini, Journal of Inorganica Chimica Acta , 2002, 338,51-58.

[42] M.A. Spackman, P.G. Byrom, Journal of Chemical Physics Letters, 1997, 267,215–220.

[43] J.J. McKinnon, A.S. Mitchell, M.A. Spackman, Journal of Chemistry - A European Journal, 1998, 4, 2136- 2141.

[44] S.K. Wolff, D.J. Grimwood, J.J. McKinnon, D. Jayatilaka, M.A. Spackamn, Crystal Explorer 3.0, University of Westren Australia, Perth, 2007.

[45] A.L. Rohl, M. Moret, W. Kaminsky, K. Claborn, J.J. Mckinnon, B. Kahr, Journal of Crystal Growth & Design,2008,8, 4517- 4525.

[46] M.A. Spackman, J.J. McKinnon, Journal of CrystEngComm, 2002, 4, 378- 392.

[47] J. Janczak, G.J. Perpetuo, J Acta Crystallographica Section C, 2001, 57,1431- 1433.

[48] R. Elwej, N. Hannachi, I. Chaabane, A. Oueslati, F. Hlel, Journal of Inorganica Chimica Acta, 2013,406 , 10- 19.

[49]R. Elwej, A. Bulou, F. Hlel, Journal of Synthetic Metals, 2016, 222,372- 382.

[50]M.Hamdi,A.Oueslati,I.Chaabane,F.Hlel,Journal of ISRN Condensed Matter Physics,2012, 750497,1-8

[51]N.Sundaraganesan,C.Meganathan,M.Kurt,Journalof Molecular Structure, 2008, *891*,284- 291.

[52] A. Kabadou, R. Ben Hassen, M. Mnif, A. Ben Salah, Journal of Alloys and Compounds, 1999,284, 128- 131.

[53] D. Massiot, H. Theile, A. Germany, WinFit—a Windows-based program for line shape analysis." *Bruker Report*,1994, 140 ,43-46.

[54] W. Wamani, R. Elwej, T. Mhiri, M. Belhouchet, Journal of Advances in Chemistry, 2013, 5,741-752.

[55] R.Hajji ,A. Oueslati, ,N. Errien, F. Hlel, Journal of *Polyhedron*,2014, *79*,97-103.

[56] H.C. Galka, L.H. Gade,Journal of Inorganica Chimica Acta,2004 ,357, 1725- 1732.

[57] R. Elwej, N. Hannachi, K. Adil, F. Hlel, Journal of Phosphorus, Sulfur, and Silicon and the Related Elements, 2012,187, 1173- 1182.

Figures caption:

Fig.1.The asymmetric unit of the compound showing the atom numbering scheme. Thermal ellipsoids are represented for non-hydrogen atoms (70%).

Fig.2. Projection of crystal of $(C_6H_{10}N_2)$ $(Hg_2Cl_5)_2$.$3H_2O$ on *ab* plane.

Fig.3. The cationic layer on *bc* plane.

Fig.4. The anionic layer on *bc* plane.

Fig.5. Intermolecular hydrogen bonds of $(C_6H_{10}N_2)(Hg_2Cl_5)_2.3H_2O$ compound.

Fig .6. Hirshfeld surface mapped with d_e d_{norm} and d_i of the title compound : d_{norm} mapped on Hirshfeld surface for visualizing the intercontacts.

Fig.7. full fingerprint ((a) -- (l)) of the title compound : di is the closest internal distance from a given point on the Hirshfeld surface and de is the closest external contacts.

Fig.8. a. Infrared and Raman spectrum of $(C_6H_{10}N_2)(Hg_2Cl_5)_2.3H_2O$

Fig. 8.b.Deconvulution of the Raman spectrum by using the LabSpec5 program of title compound $(C_6H_{10}N_2)(Hg_2Cl_5)_2.3H_2O$

Fig.9. Experimental and fitted curves of b_1; b_2 and b_3 bands.

Fig.10. DSC and TGA curves for the $(C_6H_{10}N_2)(Hg_2Cl_5)_2.3H_2O$

Tables caption:

Table. 1 : Summary of crystal data, X-rays diffraction intensity measurements and refinement parameters $(C_6H_{10}N_2)$ $(Hg_2Cl_5)_2$. $3H_2O$.

Table 2: Fractional atomic coordinates, site occupancy (%) and equivalent isotropic displacement parameters ($Å^2$).

Table 3 : Main distances (**Å**) and bond angles (°) for the organic entities of $(C_6H_{10}N_2)$ $(Hg_2Cl_5)_2$.$3H_2O$; (e.s.d. are given in parentheses).

Table 4: Main distances (**Å**) and bond angles (°) for the inorganic entities of $(C_6H_{10}N_2)$ $(Hg_2Cl_5)_2.3H_2O$; (e.s.d. are given in parentheses).

Table 5: Main inter –atomic distances (Å) and bond angles (°) involved in the hydrogen bonds of $(C_6H_{10}N_2)(Hg_2Cl_5)_2.3H_2O$.

Table 6: The combinaison d_e and d_i obtained by the 2-D fingerprint plots.

Table 7: Assignments of the observed infrared and Raman spectra of $(C_6H_{10}N_2)_2(Hg_2Cl_5)$ $3H_2O$ (**J.** in this work**)** .

Table 8: ^{13}C cross-polarization NMR MAS of $(C_6H_{10}N_2)$ $(Hg_2Cl_5)_2$. $3H_2O$ at 8kHz.

Table. 1 : Summary of crystal data, X-rays diffraction intensity measurements and refinement parameters $(C_6H_{10}N_2)$ $(Hg_2Cl_5)_2$. $3H_2O$.

Structural data

Empirical formula	$C_6\ H_{16}\ Cl_{10}\ Hg_4\ N_2\ O_3$
Extended formula	$2(Cl_5\ Hg_2)$, $C_6\ H_{10}\ N_2$, $3(H_2O)$
Formula weight	1321.07 g/mol
Temperature	150 (2) K
Wavelength	0.71073 Å
Crystal system, space group	monoclinic, *C 2/c*
Unit cell dimensions	a = 19.6830(15) Å,
	b =18.1870(15) Å, c = 6.8567(6) Å
	β = 93.224(3) °
Volume	2450.6(3) $Å^3$
Z, Calculated density	4, 3.581 $g.cm^{-3}$
Absorption coefficient	26.082 mm^{-1}
F(000)	2320
Crystal size	0.150 x 0.120 x 0.090 mm
Crystal color	colourless
Theta range for data collection	3.052 to 27.481 °
h_min, h_max	-25, 25
k_min, k_max	-23, 21
l_min, l_max	-8, 8
Reflections collected / unique	12564 - 2805 [R(int)[a] = 0.0532]
Reflections [I>2σ]	2667
Absorption correction type	multi-scan
Max. and min. transmission	0.096, 0.034
Refinement method	Full-matrix least-squares on F^2
Data / restraints / parameters	2805 / 0 / 117
[b] S (Goodness-of-fit)	1.145
Final *R* indices [I>2σ]	$R1^c$ = 0.0296, $wR2^d$ = 0.0710
R indices (all data)	$R1^c$ = 0.0318, $wR2^d$ = 0.0733
Largest diff. peak and hole	1.469 and -1.860 $e^-.Å^{-3}$

$^aR_{int} = \sum |F_o^2 - < F_o^2 >| / \sum [F_o^2]$ / $^bS = \{\sum [w(F_o^2 - F_c^2)^2] / (n - p)\}^{1/2}$ / $^cR1 = \sum ||F_o| - |F_c|| / \sum |F_o|$

$^{d}wR2 = \{\sum [w(F_o^2 - F_c^2)^2] / \sum [w(F_o^2)^2]\}^{1/2}$ / $w = 1/[\sigma(F_o^2) + aP^2 + bP]$ where $P = [2F_c^2 + MAX(F_o^2, 0)] /3$

Table 2: Fractional atomic coordinates, site occupancy (%) and equivalent isotropic displacement parameters ($Å^2$).

Atom	**X**	**Y**	**Z**	**U(eq)**
Hg1	0.30045(2)	0.55231(2)	0.32962(4)	0.01309(11)
Hg2				
Cl1	0.27697(2)	0.83275(2)	0.21764(5)	0.01720(11)
Cl2				
	0.20975(9)	0.50255(11)	0.4897(3)	0.0138(3)
	0.40494(9)	0.56962(10)	0.1997(3)	0.0151(4)
Cl3	0.23528(8)	0.68232(9)	0.2061(3)	0.0125(3)
Cl4	0.16611(8)	0.86841(10)	0.2779(3)	0.0142(4)
Cl5	0.39414(9)	0.81733(11)	0.2488(3)	0.0185(4)
N1	0.0728(3)	0.7161(3)	0.2229(9)	0.0107(12)
C2	0.0351(3)	0.6469(4)	0.2374(10)	0.0096(13)
C4	0.0348(4)	0.5148(4)	0.2373(12)	0.0159(15)
C3	0.0693(4)	0.5812(4)	0.2233(11)	0.0129(14)
O1W	0.4816(3)	0.6934(3)	0.4978(8)	0.0194(12)
O2W	0.500000	0.5758(5)	0.750000	0.026(2)

Table 3 : Main distances (**Å**) and bond angles (°) for the organic entities of $(C_6H_{10}N_2)(Hg_2Cl_5)_2 .3H_2O$; (e.s.d. are given in parentheses).

Distances (Å)		**Angles (°)**	
N1 - C2	1.467(9)	C3- C2- $C2^i$	119.80(4)
C2 - C3	1.378(10)	C3 - C2 - N1	119.20(6)
C2 - $C2^i$	1.402(13)	$C2^i$- C2 - N1	120.90(4)
C4 - C3	1.391(11)	C3 - C4- $C4^i$	119.70(4)
C4 - $C4^i$	1.392(16)	C2 - C3 - C4	120.50(7)

Symmetry transformations used to generate equivalent atoms: ^{i}-x, y, -z+1/2

Table 4: Main distances (**Å**) and bond angles (°) for the inorganic entities of $(C_6H_{10}N_2)(Hg_2Cl_5)_2.3H_2O$; (e.s.d. are given in parentheses).

Distances (Å)		**Angles (°)**	
Band distances of inorganic entities		Band angles of inorganic entities	
Hg1 - Cl1	2.3305(17)	Cl2 - Hg1 - Cl1	163.22(7)
Hg1 - Cl2	2.3084(18)	Cl2 - Hg1 - Cl3	99.85(6)
Hg1 - Cl3	2.7985(17)	Cl1 - Hg1 - Cl3	96.92(6)
Hg2 - Cl5	2.3212(18)	Cl5- Hg2 - Cl4	161.93(7)
Hg2 - Cl4	2.3353(17)	Cl5 - Hg2 - Cl3	99.75(6)
Hg2 - Cl3	2.8561(17)	Cl4 - Hg2- Cl3	90.07(6)

Table 5: Main inter –atomic distances (Å) and bond angles (°) involved in the hydrogen bonds of $(C_6H_{10}N_2)(Hg_2Cl_5)_2.3H_2O$

D-H***A	D-H (Å)	H...A (Å)	D...A (Å)	<(DHA) (°)
N1-H1A***Cl3	0.91	2.36	3.265(6)	175.6
N1-H1B***O1W^{i}	0.91	1.94	2.784(9)	154.3
N1-H1C***Cl5^{i}	0.91	2.94	3.390(7)	112.1
N1-H1C***O1W^{ii}	0.91	2.02	2.829(8)	147.1

Symmetry transformations used to generate equivalent atoms:
^{i} -x +1/2, -y+1/2, -z T= [0, 0, 0]
^{ii} x +1/2, -y+1/2, z-1/2 T= [-1, 0, 0]

Table 6: The combinaison d_e and d_i obtained by the 2-D fingerprint plots.

	min	max	mean	Mean+	Mean-	Pi	Sigma+	Sigma-	SigmaT	nu
$D_{(norm)}$	-1.1791	1.0493	0.3060	0.3832	-0.2951	0.2194	0.039703	0.084545	0.124249	0.2174
Di	0.6973	2.7738	1.8176	1.8176	nan	0.2620	0.110412	nan	nan	nan
De	0.6981	2.7692	1.8539	1.8539	nan	0.2618	0.113041	nan	nan	nan

Table 7: Assignments of the observed infrared and Raman spectra of $(C_6H_{10}N_2)_2(Hg_2Cl_5)3H_2O$ (**J.** in this work**)** .

IR wavenumbers (cm⁻1)					Raman wavenumbers (cm⁻1)						Assignments
[48]	**[31]**	**[49]**	**[50]**	**J**	**[48]**	**[14]**	**[31]**	**[49]**	**[50]**	**J**	
						56				55 , 3	Inorganic entities
						92			81	100,2	
						99				110,1	
						115					
						125			135	138,7	
						158				155,9	
						172					
										208,3	
									223	237,3	
										250,8	
						322				335,1	

						348				354	
										376,5	
	428	428		429				427	430	432	δ (C=C)
445				463	449	445	455	446			
	509	498	514	501			513	517			β (C-C-C)
555			-	525	529	544/566			565	522	β (C-C)
592	592	588	595	591	564			570		567,3	β (C-N-C)
										584	
-				689						601,4	ω (NH_2)
753 /761			761/779	750	732	729		727		738,6	γ (CH)
941	962		-	930							γ (CH)
1164	1180	1187	1186	1112							γ (C-C)
1220	1231	1224	1225	1211						1031,1	β (CH)
										1037,5	
	-	-	-	1257	1166		1188	1188	1179	1070,3	υ (C=N)
	1296	1297	1296	1290			1237	1232	1224		υ (C=N)
1292											
		-		1369	1297	1283	1296	1303	1297		*δ* (CH) + *δ* (NH) et *ν* (CN)
1384	1362	1371	1368	1473	1384		1374	1374			
1466	1471		1480	1670							υ (C=C)
1653	1659	1664	1669	2340		2911	2919				
-	-	-	-		2966			2954			
-	-	-	-	2360							υ_s (CH)
-	3195	3205	-	3157	3204		3212	3210			υ_{as} (CH)
-	-	-	-	3235			3233				υ_{as} (NH)
-	-	-	-	3280	3296						υ_s(NH)
3406		3401		3350-3400							υ_s (OH), υ_{as} (OH)
3566											

υ: Stretching; υ_s: sym stretching; υ_{as}: asym stretching; β: in- plane- bending; γ: out-of -plane bending; ω: wagging; ρ : rocking; t: twisting; τ: torsion.

Table 8: ^{13}C cross-polarization NMR MAS of $(C_6H_{10}N_2)$ $(Hg_2Cl_5)_2$. $3H_2O$ at 8kHz.

Signal	No. of peaks	Position (0.1ppm)	Width (0.1ppm)
b_1	C1	133	0.5
	C6	131	0.6
b_2	C2	129	0.5
	C5	128	0.7
b_3	C3	123	0.6
	C4	121	0.6

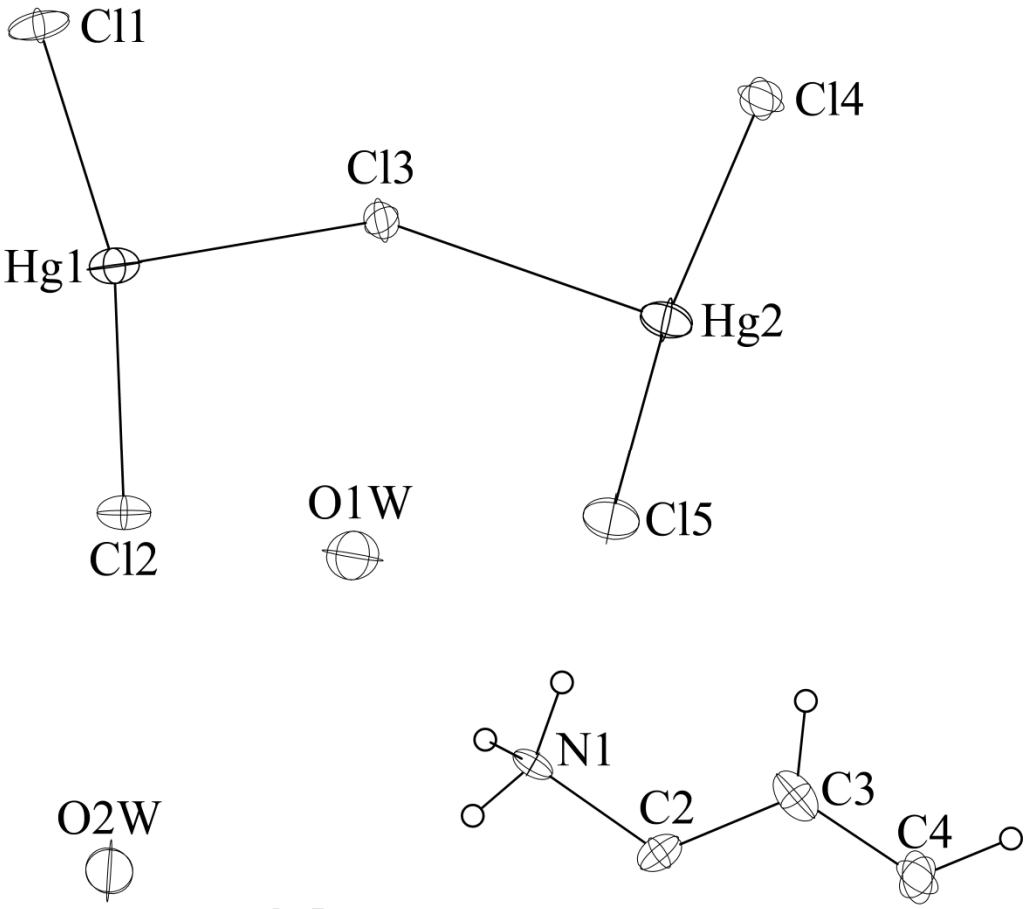

Fig.1. The asymmetric unit of the compound showing the atom numbering scheme. Thermal ellipsoids are represented for non-hydrogen atoms (70%).

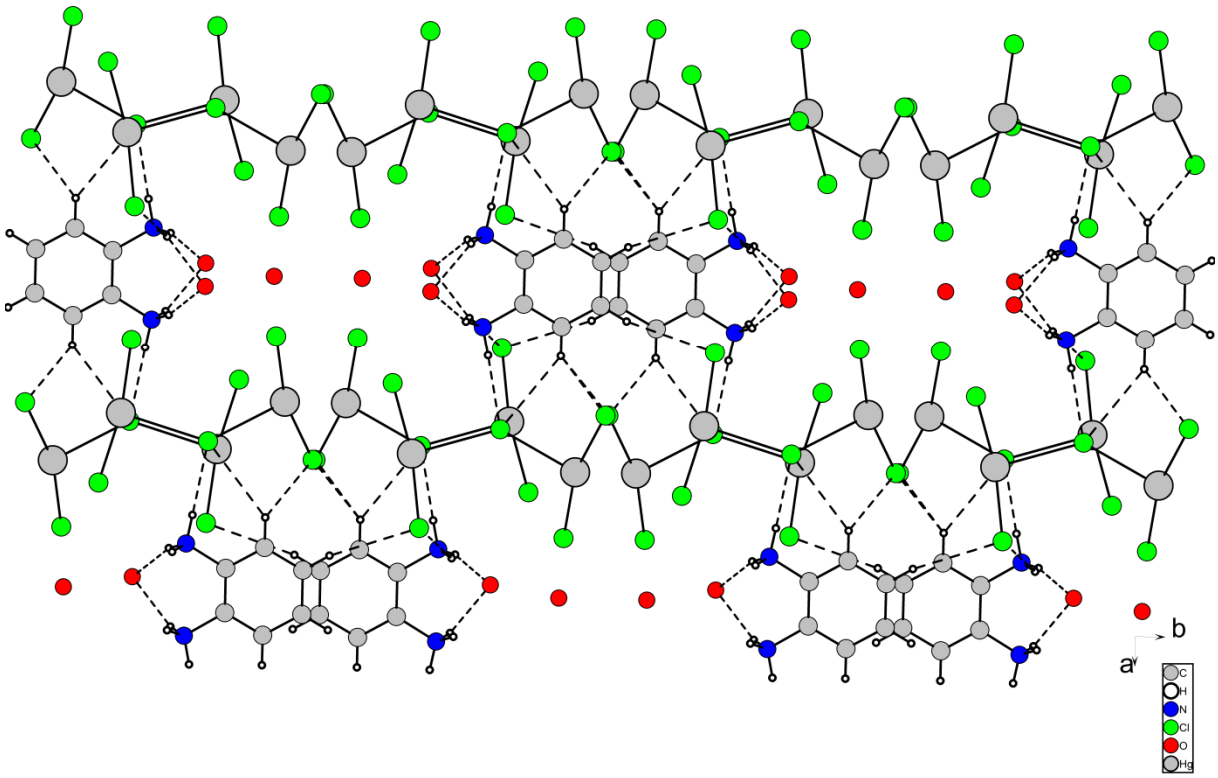

Fig.2. Projection of crystal of $(C_6H_{10}N_2)$ $(Hg_2Cl_5)_2$.$3H_2O$ on *ab* plane.

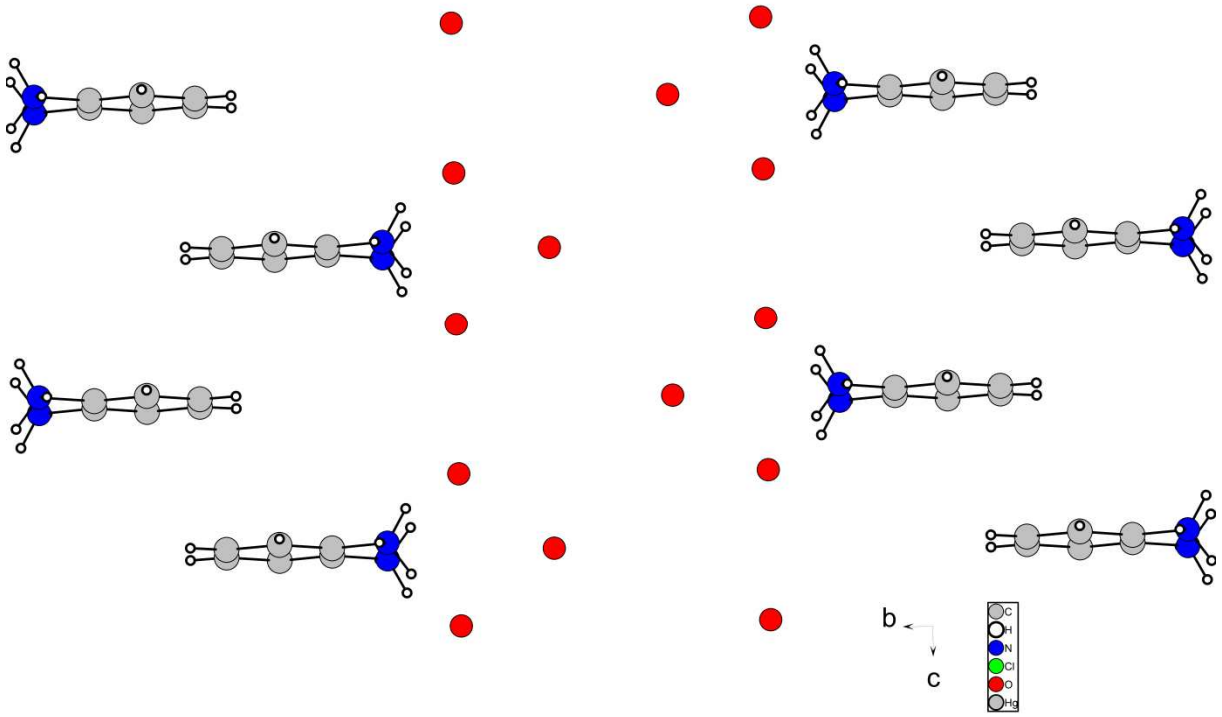

Fig.3. The cationic layer on *bc* plane

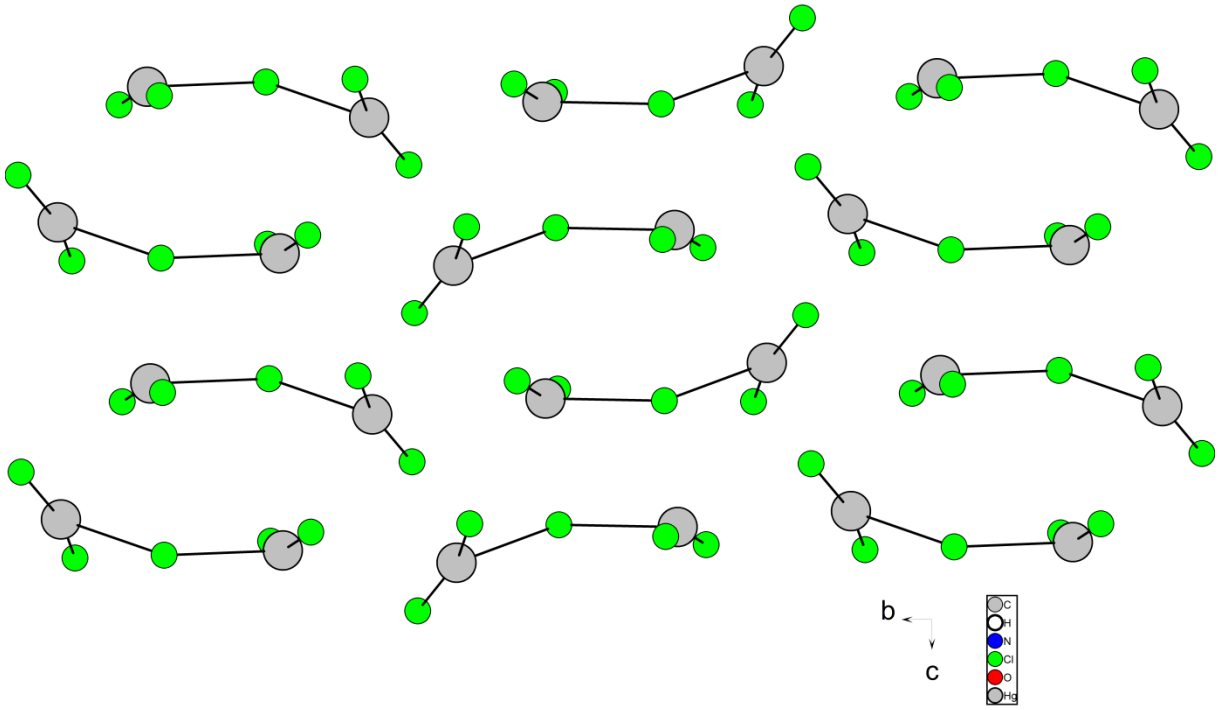

Fig.4. The anionic layer on *bc* plane

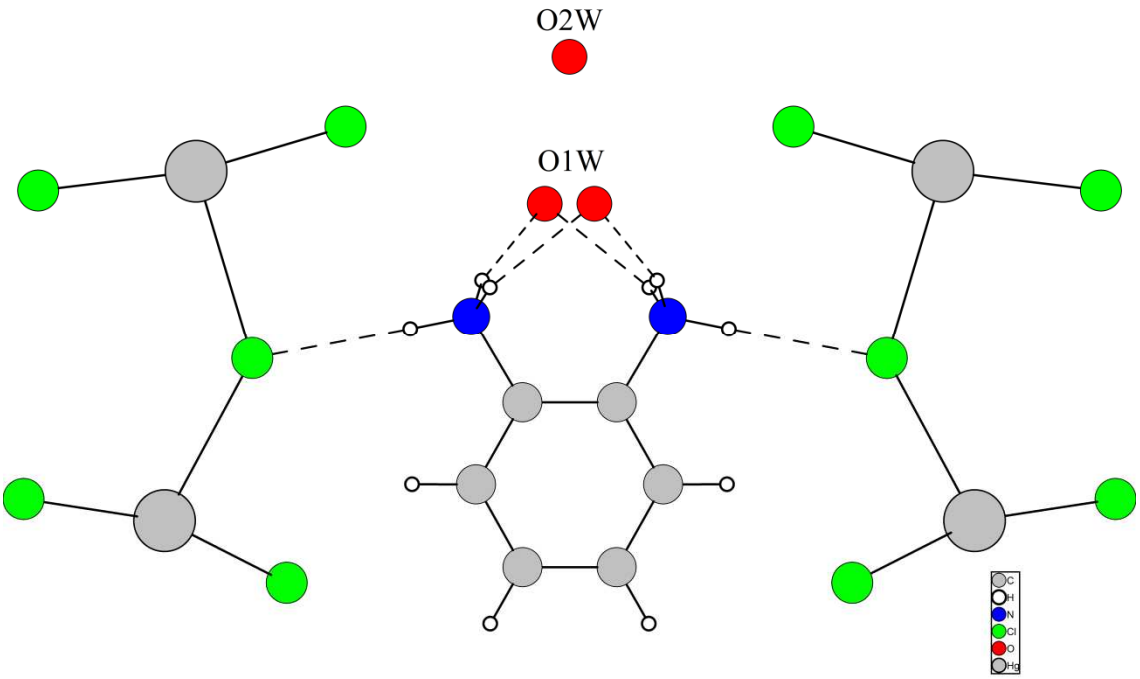

Fig.5. Intermolecular hydrogen bonds of $(C_6H_{10}N_2)(Hg_2Cl_5)_2.3H_2O$ compound.

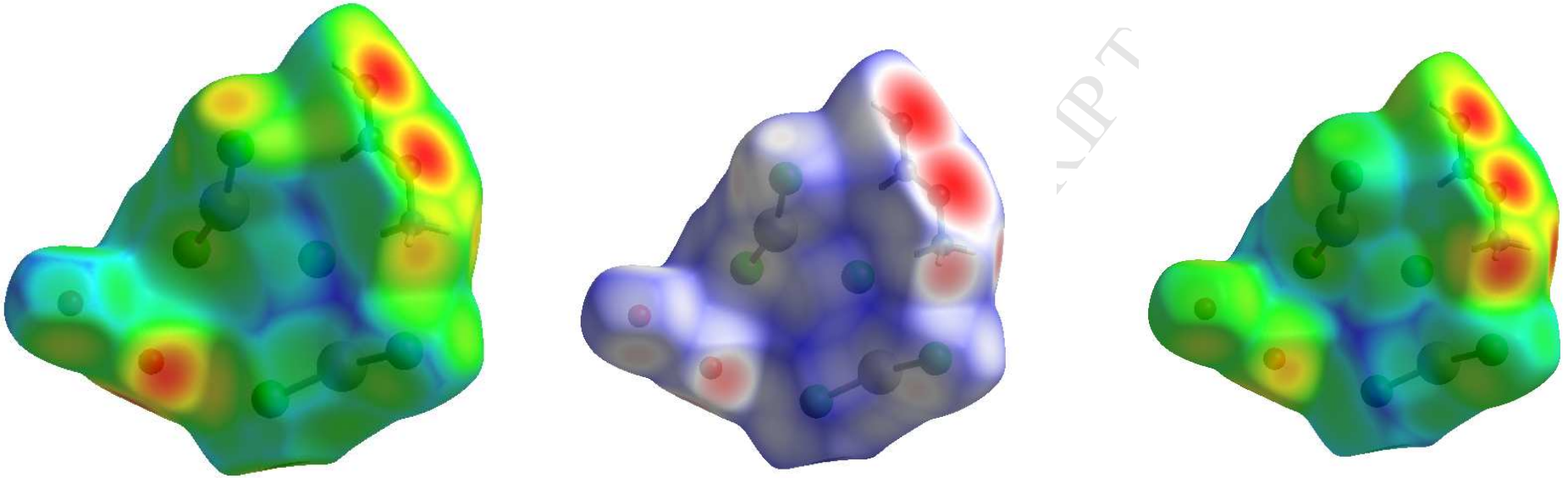

(a) **Surface d_e** **(b) Surface d_{norm}** **(c) Surface d_i**

Fig .6. Hirshfeld surface mapped with d_e d_{norm} and d_i of the title compound : d_{norm} mapped on Hirshfeld surface for visualizing the intercontacts

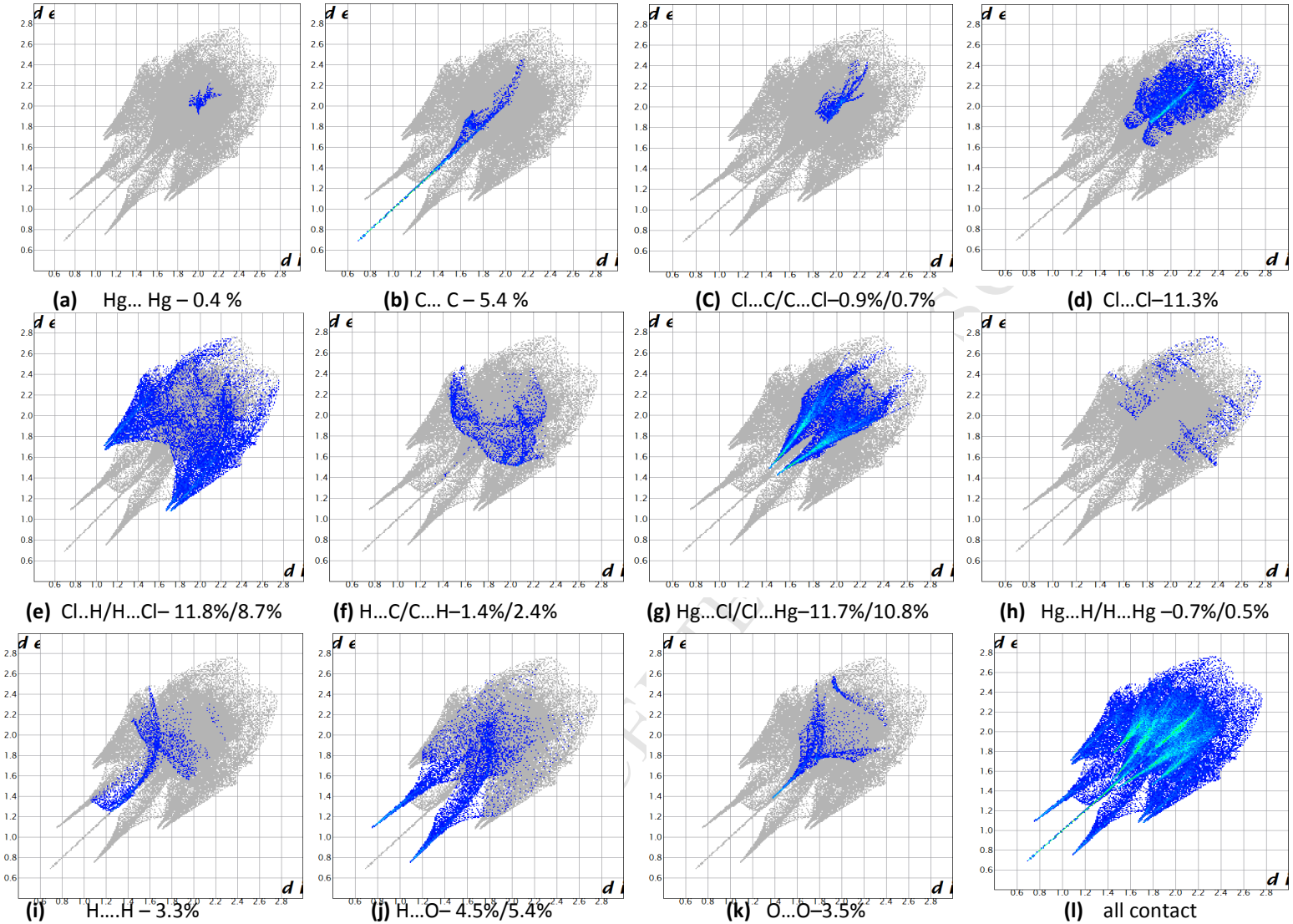

Fig.7. full fingerprint ((a) -- (l)) of the title compound : di is the closest internal distance from a given point on the Hirshfeld surface and de is the closest external contacts.

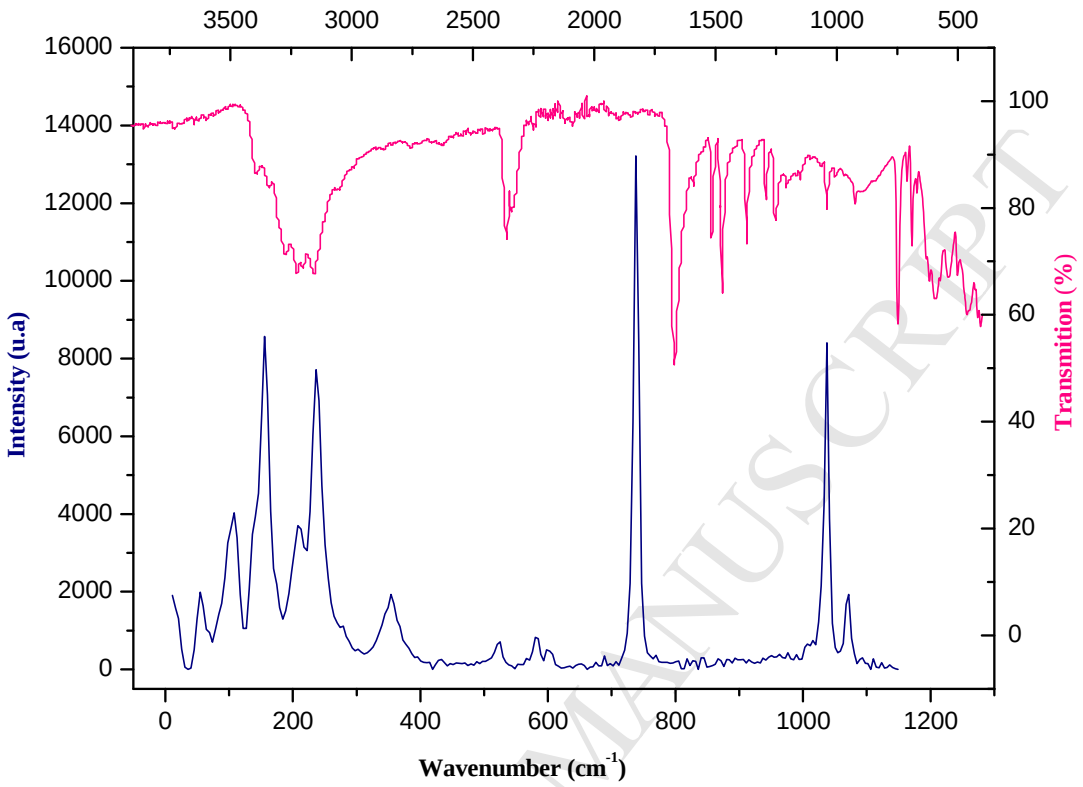

Fig.8. a. Infrared and Raman spectrum of $(C_6H_{10}N_2)(Hg_2Cl_5)_2.3H_2O$

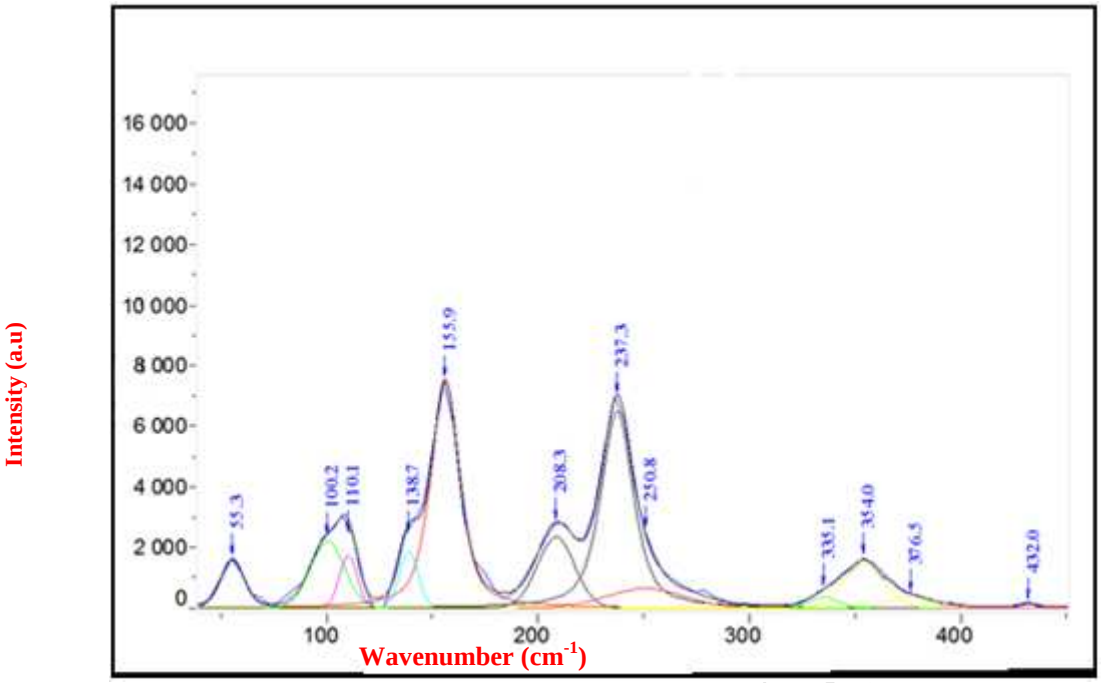

Fig. 8.b.Deconvulution of the Raman spectrum by using the LabSpec5 program of title compound $(C_6H_{10}N_2)(Hg_2Cl_5)_2.3H_2O$

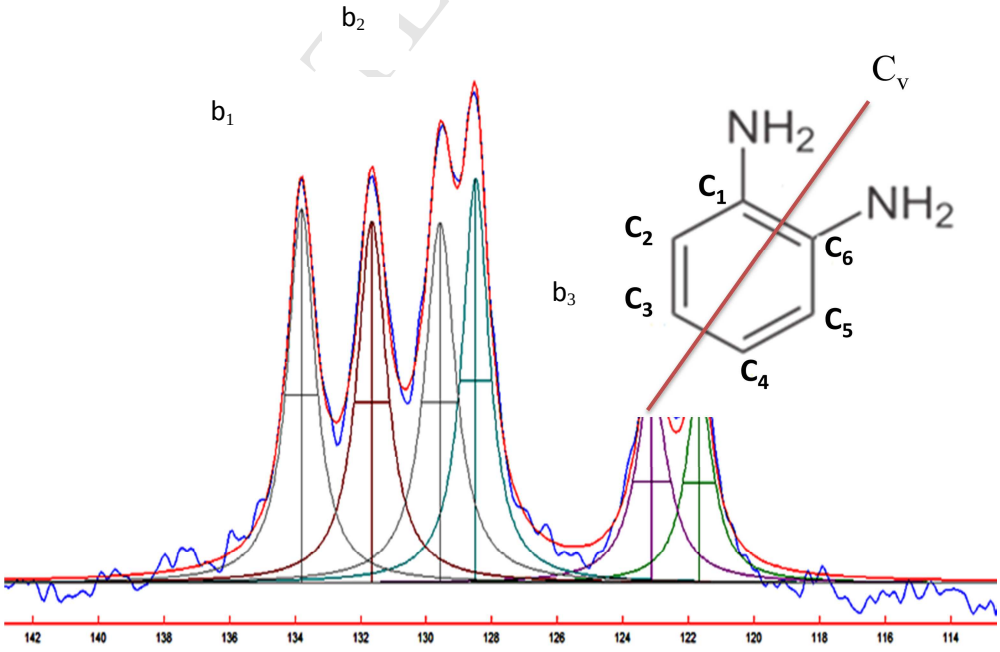

Fig.9. Experimental and fitted curves of b_1; b_2 and b_3 bands.

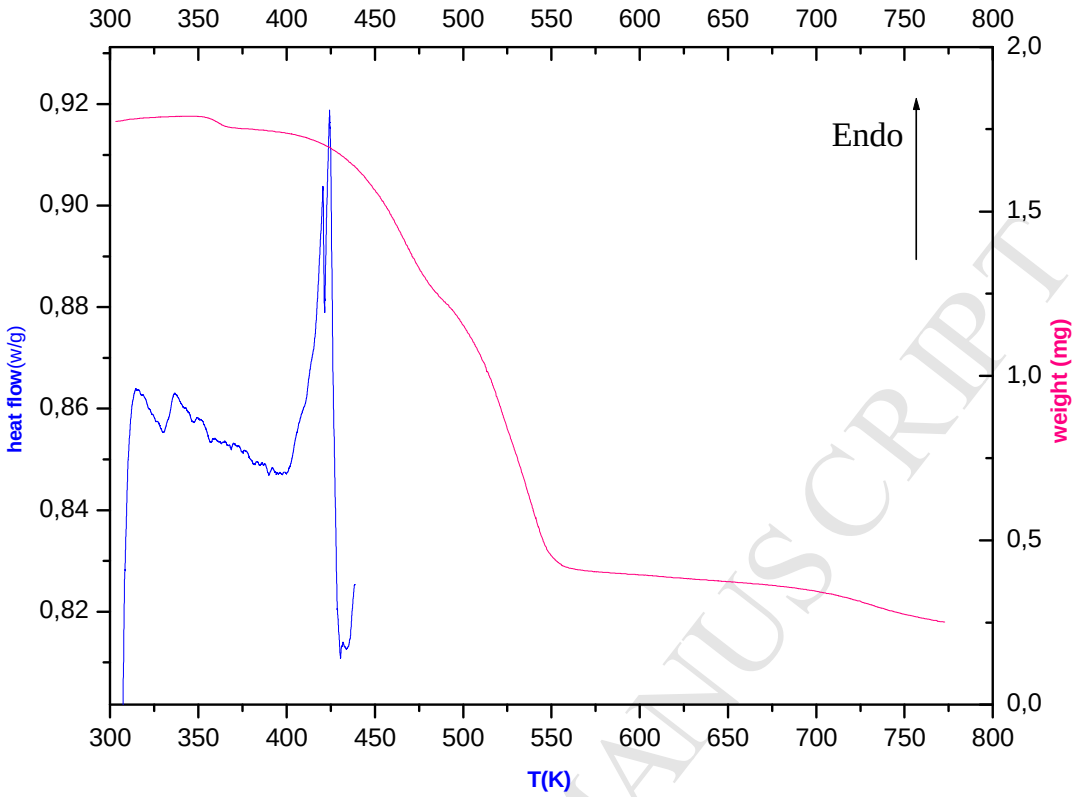

Fig.10. DSC and TGA curves for the $(C_6H_{10}N_2)(Hg_2Cl_5)_2.3H_2O$

Highlights

- New hybrid complex, $(C_6H_{10}N_2)(Hg_2Cl_5)_2.3H_2O$ was prepared by hydrothermal methods
- The atomic arrangement shows alternation of cationic and anionic layers.
- X-ray diffraction, DSC, TGA, IR, Raman and NMR studies were reported.
- The intermolecular interactions have also been analyzed by the Hirshfled surfaces analysis.